

# *Spitzer* Photometry of $\sim 1$ Million Stars in M 31 and 15 Other Galaxies <sup>1</sup>

Rubab Khan<sup>2,3</sup>

## ABSTRACT

We present *Spitzer* IRAC  $3.6 - 8 \mu\text{m}$  and MIPS  $24 \mu\text{m}$  point-source catalogs for M 31 and 15 other mostly large, star forming galaxies at distances  $\sim 3.5 - 14$  Mpc including M 51, M 83, M 101 and NGC 6946. These catalogs contain  $\sim 1$  million sources including  $\sim 859,000$  in M 31 and  $\sim 116,000$  in the other galaxies. They were created following the procedures described in Khan et al. (2015b) through a combination of point spread function (PSF) fitting and aperture photometry. These data products constitute a resource to improve our understanding of the IR-bright ( $3.6 - 24 \mu\text{m}$ ) point-source populations in crowded extragalactic stellar fields and to plan observations with the James Webb Space Telescope.

*Subject headings:* catalogs — surveys — techniques: photometric — infrared: stars — galaxies: individual (M 31, M 51, M 83, M 101, NGC 6946)

## 1. Introduction

The Infrared Array Camera (IRAC, Fazio et al. 2004) and the Multiband Imaging Photometer (MIPS, Rieke et al. 2004) instruments aboard the *Spitzer* Space Telescope (*Spitzer*, Werner et al. 2004) have collected a vast archive of mid-infrared (mid-IR) imaging data. This resource makes it feasible to identify and characterize mid-IR luminous stars in the crowded and dusty disks of large star forming galaxies despite difficulties due to IR emission from interstellar dust, blending and background contamination. In Khan et al. (2010) we published the first ever mid-IR point-source catalogs for galaxies significantly beyond the Local Group ( $\gtrsim 1.9$  Mpc). In Khan et al. (2015b) we used archival IRAC and MIPS images of seven galaxies at  $\sim 1 - 4$  Mpc to catalog  $\sim 300,000$  stars, that were used to identify an emerging class of high mass ( $> 25M_{\odot}$ ) post-main-sequence stars (Khan et al. 2015a). Here we present photometric inventories of the mid-IR point sources in the IRAC  $3.6 \mu\text{m}$ ,  $4.5 \mu\text{m}$ ,  $5.8 \mu\text{m}$  and  $8 \mu\text{m}$  as well as MIPS  $24 \mu\text{m}$  images of the Andromeda

---

<sup>1</sup>Based on observations made with the *Spitzer* Space Telescope, which is operated by the Jet Propulsion Laboratory, California Institute of Technology under a contract with NASA.

<sup>2</sup>JWST Fellow, NASA Postdoctoral Program, NASA Goddard Space Flight Center, MC 665, 8800 Greenbelt Road, Greenbelt, MD 20771

<sup>3</sup>Department of Astronomy, Box 351580, University of Washington, Seattle, WA 98195; rubab@uw.edu

galaxy (M31) and 15 other nearby ( $\lesssim 14$  Mpc) galaxies beyond the Local Group. Our key motivation here is to facilitate targeted follow-up of individual objects and observation planning of IR-bright extragalactic stellar populations in the upcoming era of the James Webb Space Telescope (JWST, Gardner et al. 2006) and the Wide-Field Infrared Survey Telescope (WFIRST, Spergel et al. 2015).

As the nearest major spiral galaxy to the Milky Way, the Andromeda galaxy (M31) have been extensively observed over the years from both ground and space based observatories (e.g., Baade 1944; de Vaucouleurs 1958; Massey et al. 2006; Johnson et al. 2012). The Panchromatic Hubble Andromeda Treasury (Dalcanton et al. 2012) mapped roughly a third of M31’s star forming disk, using 6 filters covering from the ultraviolet through the near-infrared (near-IR) to produce the most detailed picture of resolved extragalactic stellar populations in a galaxy. However, public availability of mid-IR stellar catalogs of this galaxy is very limited. Mould et al. (2008) performed mid-IR photometry of point sources on *Spitzer* IRAC and MIPS images of M31. However, while their paper shows mid-IR color magnitude diagrams containing seemingly many hundred thousand sources, they published only a small fraction ( $\sim 500 - 900$  sources at various bands) of the catalog, consisting of the brightest sources in the field. In this paper, we present an extensive mid-IR point-source catalog of M31 consisting of  $\sim 859,000$  sources, covering the entirety of M31’s disk including the accompanying M32 and M110 galaxies.

When selecting the other 15 galaxies, we concentrated on those with higher recent star formation rate (SFR), as these would have large numbers of short lived, massive, evolved mid-IR bright stars, and we cataloged  $\sim 116,000$  stars in these galaxies. These catalogs include the highly star-forming galaxies M83, NGC 6946, M101 and M51 (M51a and M51b) which enabled the first-ever identification of extragalactic candidate analogs of the Galactic stellar behemoth  $\eta$  Carinae (Khan et al. 2015c). We selected these 15 galaxies to span a range of distances and SFRs ( $\sim 3.5 - 14$  Mpc and  $\lesssim 0.1 - \sim 1M_{\odot}$ /year, see Table 1), and currently there are no public mid-IR stellar catalogs for 13 of these galaxies. Williams et al. (2015) published a mid-IR bright source catalog of M83 including *Spitzer* 3.6 and 4.5  $\mu\text{m}$  band measurements for  $< 4,000$  objects, while the M83 catalog presented here contains *Spitzer* 3.6, 4.5, 5.8, 8 and 24  $\mu\text{m}$  band measurements for  $\sim 23,000$  sources. Likewise, Khan et al. (2010) reported two *Spitzer* band measurements of  $< 6,000$  objects in NGC 6946 whereas the catalog for this galaxy presented here contains five *Spitzer* band measurements for  $\sim 16,000$  sources.

For M31, we used the IRAC 3.6  $\mu\text{m}$ , 4.5  $\mu\text{m}$ , 5.8  $\mu\text{m}$  and 8  $\mu\text{m}$  mosaics produced by Mould et al. (2008) and the MIPS 24  $\mu\text{m}$  mosaic produced by Gordon et al. (2006). For the other galaxies, we used the IRAC and MIPS mosaics produced by the *Spitzer* Infrared Nearby Galaxies Survey (SINGS, Kennicutt et al. 2003) and the Local Volume Legacy Survey (LVL, Dale et al. 2009). We utilize the full mosaics available for each galaxy. The M31 mosaics (covering  $\sim 4.2$  square degrees) are constructed from many individual exposures whereas each of the more distant galaxy images from the LVL and SINGS archives are usually combinations of two slightly offset images. We do not take advantage of the uncertainty maps and assume mean noise properties, since in

our experience the dominant source of flux uncertainty in this context are related to crowding, which varies significantly across face of the target galaxies. In what follows, we summarize our methodology (Section 2, see Khan et al. (2015b) for details), and discuss properties of the catalogs and color-magnitude distributions (Section 3).

## 2. Photometry

We obtained the photometric measurements at various wavelengths and combined them to construct the point-source catalogs following the procedures established in Khan et al. (2015b). We implement a strict detection criteria by requiring  $> 3\sigma$  detection of all cataloged sources at  $3.6\ \mu\text{m}$  and  $4.5\ \mu\text{m}$ . We then complement those measurements at the  $5.8\ \mu\text{m}$ ,  $8.0\ \mu\text{m}$  and  $24\ \mu\text{m}$  bands through a combination of point spread function (PSF) fitting photometry and aperture photometry. For all objects that do not have a  $> 3\sigma$  detection at these three longer wavelengths, we estimate their  $3\sigma$  flux upper limits in those bands.

First we select all sources detected through PSF fitting photometry at  $> 3\sigma$  in both the  $3.6\ \mu\text{m}$  and  $4.5\ \mu\text{m}$  images within a 1 pixel matching radius as point sources. Next, we search for  $> 3\sigma$  detections of these point sources in the  $5.8\ \mu\text{m}$  and  $8.0\ \mu\text{m}$  images within the same matching radius. If no counterpart is found, we attempt to measure the flux at the location of the  $3.6/4.5\ \mu\text{m}$  point source through PSF fitting, and failing that, through aperture photometry. For the MIPS  $24\ \mu\text{m}$  images, we only use aperture photometry due to the much lower resolution and larger PSF size compared to the IRAC images<sup>4,5,6</sup>. Finally, for all objects that do not have a  $> 3\sigma$  detection at  $5.8\ \mu\text{m}$ ,  $8.0\ \mu\text{m}$  and  $24\ \mu\text{m}$ , we estimate the  $3\sigma$  flux upper limits. The fluxes and upper limits are transformed to Vega-calibrated magnitudes using the flux zero-points and aperture corrections provided in the *Spitzer* Data Analysis Cookbook<sup>7</sup>.

We used the DAOPHOT/ALLSTAR PSF-fitting and photometry package (Stetson 1992) to construct the PSFs, to identify the  $> 3\sigma$  sources and to measure their flux at all 4 IRAC bands. We used the IRAF<sup>8</sup> ApPhot/Phot tool for performing aperture photometry for all IRAC bands and the MIPS  $24\ \mu\text{m}$  band. For the four IRAC bands, we use an extraction aperture of  $2''.4$ , a local background annulus of  $2''.4 - 7''.2$  and aperture corrections of 1.213, 1.234, 1.379, and 1.584 respectively. For the MIPS  $24\ \mu\text{m}$  band, we use an extraction aperture of  $3''.5$ , a local background

---

<sup>4</sup>Mean full width half-max (FWHM) of the cryogenic IRAC PSFs are  $1''.66$ ,  $1''.72$ ,  $1''.88$  and  $1''.98$ , and the MIPS  $24\ \mu\text{m}$  PSF FWHM is  $5''.9$ .

<sup>5</sup><http://irsa.ipac.caltech.edu/data/SPITZER/docs/irac/iracinstrumenthandbook/5/>

<sup>6</sup><http://irsa.ipac.caltech.edu/data/SPITZER/docs/mips/mipsinstrumenthandbook/50/>

<sup>7</sup><http://irsa.ipac.caltech.edu/data/SPITZER/docs/dataanalysistools/>

<sup>8</sup>IRAF is distributed by the National Optical Astronomy Observatory, which is operated by the Association of Universities for Research in Astronomy (AURA) under cooperative agreement with the National Science Foundation.

annulus of  $6'' - 8''$  and an aperture correction of 2.78. We estimate the local background using a  $2\sigma$  outlier rejection procedure in order to exclude sources located in the local sky annulus and correct for the excluded pixels assuming a Gaussian background distribution. We determine the  $3\sigma$  flux upper limit for each aperture location using the local background estimate.

We present the results of our mid-IR photometric survey following the same format as the catalogs published in Khan et al. (2015b). Tables 2–17 list the coordinates (J2000.0; RA and Dec) of the point sources followed by their Vega calibrated apparent magnitudes ( $m_\lambda$ ), the associated  $1\sigma$  uncertainties ( $\sigma_\lambda$ ) and (for the  $3.6 - 8.0\mu\text{m}$  bands) the differences between the PSF and aperture photometry magnitudes ( $\delta_\lambda$ ). For the  $5.8\mu\text{m}$ ,  $8.0\mu\text{m}$  and  $24\mu\text{m}$  bands,  $\sigma_\lambda = 99.99$  implies that the associated photometric measurement is a  $3\sigma$  flux upper limit, and  $m_\lambda = 99.99$  (as well as  $\sigma_\lambda = 99.99$ ) indicates that no reliable photometric measurement could be obtained for that location. For the IRAC bands,  $\delta_\lambda = 99.99$  implies that one or both of the associated photometric measurements did not yield a  $> 3\sigma$  flux measurement.

Large mismatches between the two (PSF-fitting and aperture) measurements, specially when  $|\delta_\lambda| \gg \sigma_\lambda$ , are a good indicator of when crowding is significantly effecting the photometry and can be useful as an alternative estimate of photometric uncertainty. While PSF-fitting photometry may be generally preferable for crowded field photometry where possible, the  $\delta_\lambda$  values would let one revert to using the aperture photometry measurements instead. Large  $\delta_\lambda$  values associated with seemingly bright sources are also indicative of contamination due to saturated foreground objects being resolved into multiple bright sources by the PSF-fitting point source detection procedure (foreground giants would have  $m \lesssim 7$ , e.g., McQuinn et al. 2007). This is a major source of false positives, specially for M 31, as its large field of view contains numerous foreground objects. Indeed, our attempt to identify evolved dust-obscured very high-mass stars ( $M_{ZAMS} \gtrsim 25M_\odot$ ) in M 31 following the selection criteria described in Khan et al. (2013) picked up many such spurious sources due to their apparently peculiar spectral energy distributions (SEDs).

### 3. Discussion

Figure 1 shows the  $m_{4.5}$  vs.  $m_{3.6} - m_{4.5}$  color magnitude diagram (CMD) for M 31 and Figure 2 shows the same for the galaxies M 83, NGC 6946, M 101 and M 51 which have the highest SFR among all the galaxies surveyed. The  $1\sigma$  color and magnitude uncertainties indicate that the horizontal extent of the CMDs are largely a result of color uncertainties. The blue-ward extent of the M 31 CMD is consistent with, e.g, the comparable CMDs of M 33 shown on Fig. 14 of McQuinn et al. (2007) and Fig. 4 of Khan et al. (2015b), and it contains a larger fraction of blue sources than the 15 galaxies beyond the local group cataloged here. As these galaxies are between factors of  $\sim 4.5$  (NGC 3077 at 3.7 Mpc) and  $\sim 18$  (NGC 3184 at 14.4 Mpc) farther away than M 31 (at 0.78 Mpc), in M 31 we identify intrinsically fainter and lower mass stars with relatively bluer colors. These include O- and C-rich Asymptotic Giant Branch (AGB) stars (e.g., Bolatto et al. 2007) and possibly some Red Giant Branch (RGB) stars ( $m_{4.5} \lesssim 18$  in M 31, e.g., Blum et al. 2006; Boyer et al. 2015) as

well as the more evolved and more luminous (massive) stars with warm circumstellar dust which have redder mid-IR colors (M 31 is known to have some young massive stars, e.g., Lewis et al. 2015; Massey et al. 2016).

All normal stars have the same mid-IR color in the first two IRAC bands, because of the Rayleigh-Jeans tails of their spectra, and we see this as a sequence of foreground dwarfs with  $m_{3.6} - m_{4.5} \simeq 0$  on the M 31 CMD, as well as a “plume” of bright and red extreme Asymptotic Giant Branch (ex-AGB) stars (Thompson et al. 2009; Khan et al. 2010; Boyer et al. 2015) at  $m_{4.5} \simeq 13 - 16$ . This feature is not as prominent on the M 31 CMD when compared to the tight stream of ex-AGB stars visible on the CMD of M 33, which has significantly higher ( $\gtrsim 10\times$ ) specific star formation rate (e.g., see Lewis et al. 2015, for a detailed discussion of M 31’s recent star formation history) and thus a larger number of younger massive stars per unit stellar mass, although it is still a prominent feature when compared to CMDs of even lower mass/SFR galaxies such as NGC 6822 (see Fig. 4 of Khan et al. 2015b for M 33 and NGC 6822 mid-IR CMDs).

However, quasars also have this color (e.g., Stern et al. 2005), as do star forming galaxies with strong PAH emission at  $8.0\mu\text{m}$  (e.g., the SED models in Assef et al. 2010), and the ex-AGB stars are far less noticeable amid background contaminants on the more distant galaxy CMDs. Although these galaxies have smaller effective survey areas and do not have more background contamination per unit area than M 31, their greater distance modulus ( $\mu$ ) means that stars in those galaxies have larger apparent magnitudes. As a result, the evolved stellar populations in those galaxies are effectively buried among background sources on the CMDs. For example, the tip of the AGB branch that is at  $m_{4.5} \simeq 13$  on the M 31 CMD ( $\mu \simeq 24.5$ , Figure 2) would be at  $m_{4.5} \simeq 17$  on the M 83 CMD ( $\mu \simeq 28.3$ , Figure 2). Given the rarity of ex-AGB stars (e.g., Thompson et al. 2009; Khan et al. 2010; Boyer et al. 2015) it is very likely that most of the very red ( $m_{3.6} - m_{4.5} \gtrsim 1$ ) sources we identify are background contaminants. However, verifying the nature of individual sources would require mid-IR variability study and/or construction of extended multi-wavelength SEDs on a case-by-case basis (e.g., Khan et al. 2013). Indeed, only a rare few cataloged mid-IR sources in these distant galaxies would be relevant in the context of studying properties of individual stars — but that is what makes them very interesting to analyze (e.g., Khan et al. 2015c).

Figure 3 shows the apparent magnitude histograms of all sources in the catalog of M 31 (clear region) as well as in the other galaxies (shaded region). For a qualitative comparison, we also show the magnitude histogram for all sources in a  $6 \text{ deg}^2$  region of the NOAO Bootes Field produced from the *Spitzer* Deep Wide Field Survey (SDWFS, Ashby et al. 2009) data (dotted line). The SDWFS catalog can be largely considered “empty” as in most sources being background galaxies and quasars, with only a small fraction being foreground stars (e.g., see Kozłowski 2016). Figure 3 shows that our catalogs are  $\gtrsim 1$  mag deeper than the SDWFS catalog. It is worth noting that our catalogs simply inventory all the sources present on the image mosaics and we do not attempt to distinguish between sources physically associated with the galaxies and unrelated foreground and background contaminants. We cannot claim completeness at any magnitude limit, rather can only infer that the observed luminosity function turns over at a certain magnitude while the intrinsic

one continues rising as the catalogs become increasingly incomplete for fainter sources. Overall, Figure 3 qualitatively implies that our source lists become significantly incomplete at  $m_{3.6} \gtrsim 18$ ,  $m_{4.5} \gtrsim 18$ ,  $m_{5.8} \gtrsim 17$  and  $m_{8.0} \gtrsim 16$ .

As we emphasized in Khan et al. (2015b), point-source catalogs of the inherently crowded galaxy fields that we are surveying are bound to be crowding (confusion) limited, not just magnitude limited. While Figure 3 empirically demonstrates that our source detection peaks at a certain magnitude and then falls off rapidly, it is likely that incompleteness is affecting even the bright-star counts in crowded regions, increasing towards and through the peak. The depth and completeness of the catalogs vary across each galaxy between, e.g., the centers of galaxies compared to their outer regions or in dusty star clusters compared to more sparsely populated regions as a function of crowding, and they can only be characterized locally for small regions. Performing a conventional efficiency determination test through addition of randomly distributed artificial objects in the images therefore would lead us to either overestimate or underestimate the efficiency. For such a study to be truly useful, it would require a proper “star-star correlation function” to be employed for spatial distribution of artificial stars. Also, while we execute the point source detection procedures in individual bands, a source is included in the catalog only if it is independently identified as a point-source in both the 3.6 and 4.5  $\mu\text{m}$  bands at least at a  $3\sigma$  level by PSF fitting. Any meaningful statistical test in this context therefore would also need to account for stellar SED variations in the mid-IR to test multi-band catalog completeness for a particular region of interest.

Figure 4 shows the mid-IR color histograms of all sources in the catalogs with  $1\sigma$  uncertainty in color  $\lesssim 0.2$ , following the same representation as Figure 3. As discussed earlier in this section, the  $m_{3.6} - m_{4.5}$  color distribution of M 31 is skewed blue-ward compared to the other galaxies. The  $m_{3.6} - m_{5.8}$  and  $m_{4.5} - m_{5.8}$  color distributions (middle row of Figure 4) of these more distant galaxies peak at  $> 1$  mag redder relative to M 31 and the Bootes field, indicating that their 5.8  $\mu\text{m}$  flux may be dominated by PAH emissions, which is a common feature of massive star-forming regions and star clusters (e.g., Churchwell et al. 2006) created by strong stochastic emission from PAH molecules (e.g., Whelan et al. 2011) excited by UV radiation from O- and B-type stars (see Wood et al. 2008 for a detailed treatment of this topic). Their  $m_{3.6} - m_{8.0}$ ,  $m_{4.5} - m_{8.0}$  and  $m_{5.8} - m_{8.0}$  color distributions generally match those of the Bootes field but are redder than M 31 (bottom row of Figure 4), consistent with significant extragalactic contamination (see Fig. 5 of Khan et al. 2015b for mid-IR CMDs of the SDWFS sources).

It is important to highlight here that the color histograms do not include sources for which we could only measure a flux upper-limits at the 5.8 and/or 8.0  $\mu\text{m}$  bands. Since the catalogs list sources that have  $> 3\sigma$  detections at the 3.6 and 4.5  $\mu\text{m}$ , the middle and bottom rows of Figure 4 are inherently biased toward redder sources, i.e., those with  $> 3\sigma$  detections at the two longer wavelength bands as well as the two shorter ones. This can exclude relatively bluer sources such as foreground dwarfs as well as O- and C-rich AGB stars in the targeted galaxies that are intrinsically less luminous at the longer wavelengths. A more rigorous pursuit of this topic requires studying near-IR to mid-IR color separations of the cataloged sources, e.g., as done for the LMC

by Blum et al. (2006) utilizing 2MASS data. However, 2MASS is not deep enough to study stellar populations in other galaxies (even M31’s distance modulus is  $\sim 6$  mags larger than the LMC’s) and one would need (e.g.) WFIRST’s Wide Field Instrument (WFI, Spergel et al. 2015) near-IR imaging data for this purpose.

These catalogs are a resource to improve our understanding of the  $3.6 - 24 \mu\text{m}$  bright point-source populations in crowded extragalactic fields and they are also an archive for studying future mid-IR transients. The JWST’s Near-IR Spectrograph (NIRSpec, Dorner et al. 2016) and Mid-IR Instrument (MIRI, Rieke et al. 2015) will cover the  $\sim 1 - 5 \mu\text{m}$  and  $\sim 5 - 28 \mu\text{m}$  wavelength ranges respectively, but the JWST’s small field of view and anticipated over-subscription practically means that these catalogs will continue to be the most detailed listing of mid-IR source properties in nearby galaxies in the near future. These  $3.6 - 24 \mu\text{m}$  point-source catalogs can be very useful to identify scientifically interesting sources for photometric and spectroscopic follow-up with NIRSpec and MIRI in general. They create a pathway for the exploration of extragalactic evolved stellar populations as well as other mid-IR bright sources with the JWST and WFIRST, making optimal and efficient use of these flagship observatories.

We thank the referee for helpful suggestions, Krzysztof Stanek, Christopher Kochanek and George Sonneborn for productive discussions, and Martha Boyer and Karl Gordon for providing the M31 image mosaics. This work is based on observations made with the *Spitzer* Space Telescope, which is operated by the Jet Propulsion Laboratory, California Institute of Technology under a contract with the National Aeronautics and Space Administration (NASA). We extend our gratitude to the SINGS Legacy Survey and the LVL Survey for making their data publicly available. This research has made use of NED, which is operated by the JPL and Caltech, under contract with NASA and the HEASARC Online Service, provided by NASA’s GSFC. RK is supported through a JWST Fellowship hosted by the Goddard Space Flight Center and awarded as part of the NASA Postdoctoral Program operated by the Oak Ridge Associated Universities on behalf of NASA.

## REFERENCES

- Ashby, M. L. N., Stern, D., Brodwin, M., et al. 2009, ApJ, 701, 428
- Assef, R. J. et al. 2010, ApJ, 713, 970
- Barmby, P., Ashby, M. L. N., Bianchi, L., et al. 2006, ApJ, 650, L45
- Baade, W. 1944, ApJ, 100, 137
- Blum, R. D., Mould, J. R., Olsen, K. A., et al. 2006, AJ, 132, 2034
- Bolatto, A. D., Simon, J. D., Stanimirović, S., et al. 2007, ApJ, 655, 212
- Boyer, M. L., McQuinn, K. B. W., Barmby, P., et al. 2015, ApJ, 800, 51

- Churchwell, E. et al. 2006, *ApJ*, 649, 759
- Dalcanton, J. J., Williams, B. F., Lang, D., et al. 2012, *ApJS*, 200, 18
- Dale, D. A. et al. 2009, *ApJ*, 703, 517
- de Vaucouleurs, G. 1958, *ApJ*, 128, 465
- Dorner, B., Giardino, G., Ferruit, P., et al. 2016, arXiv:1606.05640
- Fazio, G. G., Hora, J. L., Allen, L. E., et al. 2004, *ApJS*, 154, 10
- Ferrarese, L., Mould, J. R., Kennicutt, R. C., Jr., et al. 2000, *ApJ*, 529, 745
- Freedman, W. L., Madore, B. F., Gibson, B. K., et al. 2001, *ApJ*, 553, 47
- Gardner, J. P. et al. 2006, *SSR*, 123, 485
- Gordon, K. D., Bailin, J., Engelbracht, C. W., et al. 2006, *ApJ*, 638, L87
- Herrmann, K. A., Ciardullo, R., Feldmeier, J. J., & Vinciguerra, M. 2008, *ApJ*, 683, 630-643
- Jacobs, B. A., Rizzi, L., Tully, R. B., et al. 2009, *AJ*, 138, 332
- Johnson, L. C., Seth, A. C., Dalcanton, J. J., et al. 2012, *ApJ*, 752, 95
- Kennicutt, Jr., R. C. 1998, *ApJ*, 498, 541
- Kennicutt, Jr., R. C. et al. 2003, *PASP*, 115, 928
- . 2008, *ApJS*, 178, 247
- Khan, R., Stanek, K. Z., Prieto, J. L., et al. 2010, *ApJ*, 715, 1094
- Khan, R., Stanek, K. Z., & Kochanek, C. S. 2013, *ApJ*, 767, 52
- Khan, R., Kochanek, C. S., Stanek, K. Z., & Gerke, J. 2015a, *ApJ*, 799, 187
- Khan, R., Stanek, K. Z., Kochanek, C. S., & Sonneborn, G. 2015b, *ApJS*, 219, 42
- Khan, R., Adams, S. M., Stanek, K. Z., Kochanek, C. S., & Sonneborn, G. 2015c, *ApJ*, 815, L18
- Kozłowski, S. 2016, *ApJ*, 826, 118
- Lewis, A. R., Dolphin, A. E., Dalcanton, J. J., et al. 2015, *ApJ*, 805, 183
- Massey, P., Olsen, K. A. G., Hodge, P. W., et al. 2006, *AJ*, 131, 2478
- Massey, P., Neugent, K. F., & Smart, B. M. 2016, *AJ*, 152, 62
- McQuinn, K. B. W., Woodward, C. E., Willner, S. P., et al. 2007, *ApJ*, 664, 850



- Mould, J., Barmby, P., Gordon, K., et al. 2008, *ApJ*, 687, 230-241
- Rieke, G. H., Young, E. T., Engelbracht, C. W., et al. 2004, *ApJS*, 154, 25
- Rieke, G. H., Wright, G. S., Böker, T., et al. 2015, *PASP*, 127, 584
- Rozanski, R., & Rowan-Robinson, M. 1994, *MNRAS*, 271, 530
- Saha, A. et al. 2006, *ApJS*, 165, 108
- Sahu, D. K. et al. 2006, *MNRAS*, 372, 1315
- Shappee, B. J., & Stanek, K. Z. 2011, *ApJ*, 733, 124
- Silbermann, N. A., Harding, P., Madore, B. F., et al. 1996, *ApJ*, 470, 1
- Spergel, D., Gehrels, N., Baltay, C., et al. 2015, arXiv:1503.03757
- Stanek, K. Z., & Garnavich, P. M. 1998, *ApJ*, 503, L131
- Stern, D. et al. 2005, *ApJ*, 631, 163
- Stetson, P. B. 1992, *Astronomical Data Analysis Software and Systems I*, 25, 297
- Thompson, T. A., Prieto, J. L., Stanek, K. Z., et al. 2009, *ApJ*, 705, 1364
- Tully, R. B., Rizzi, L., Shaya, E. J., et al. 2009, *AJ*, 138, 323
- Werner, M. W., Roellig, T. L., Low, F. J., et al. 2004, *ApJS*, 154, 1
- Whelan, D. G., Johnson, K. E., Whitney, B. A., Indebetouw, R., & Wood, K. 2011, *ApJ*, 729, 111
- Williams, S. J., Bonanos, A. Z., Whitmore, B. C., Prieto, J. L., & Blair, W. P. 2015, *A&A*, 578, A100
- Wood, K., Whitney, B. A., Robitaille, T., & Draine, B. T. 2008, *ApJ*, 688, 1118

Table 1: Catalog Statistics

Galaxy	Galactic coor.		Distance	Data	SFR <sup>a</sup>	Number	
	<i>longitude</i>	<i>latitude</i>	(Mpc)	<i>reference</i>	Source	$M_{\odot}/\text{year}$	of Sources
M 31	121.174	−21.573	0.78	Stanek & Garnavich (1998)	<i>Note</i> <sup>b</sup>	0.7 <sup>c</sup>	859, 165
NGC 3077	141.899	41.659	3.7	Jacobs et al. (2009)	LVL <sup>d</sup>	0.076	3, 794
NGC 1313	283.359	−44.643	4.4	Jacobs et al. (2009)	LVL <sup>d</sup>	0.316	6, 972
NGC 5236	314.584	31.973	4.61	Saha et al. (2006)	LVL <sup>d</sup>	1.411	23, 331
NGC 4736	123.363	76.007	4.66	Jacobs et al. (2009)	SINGS <sup>e</sup>	0.224	10, 264
NGC 4826	315.680	84.423	4.66	Jacobs et al. (2009)	SINGS <sup>e</sup>	0.355	5, 137
NGC 5068	311.487	41.376	5.45	Herrmann et al. (2008)	LVL <sup>d</sup>	0.524	4, 568
NGC 6946	95.719	11.673	5.7	Sahu et al. (2006)	SINGS <sup>e</sup>	2.289	15, 813
NGC 5474	64.301	22.933	6	Rozanski & Rowan-Robinson (1994)	SINGS <sup>e</sup>	0.115	991
NGC 5457	102.037	59.771	6.43	Shappee & Stanek (2011)	LVL <sup>d</sup>	1.697	16, 291
NGC 45	55.903	−80.672	6.6	Jacobs et al. (2009)	LVL <sup>d</sup>	0.245	4, 321
NGC 5194	104.851	68.561	8	Ferrarese et al. (2000)	SINGS <sup>e</sup>	1.512	8, 601
NGC 2903	208.711	44.540	8.55	Tully et al. (2009)	LVL <sup>d</sup>	0.932	5, 579
NGC 925	144.885	−25.174	9.3	Silbermann et al. (1996)	SINGS <sup>e</sup>	0.562	4, 217
NGC 3627	241.961	64.418	10.5	Freedman et al. (2001)	LVL <sup>d</sup>	1.022	3, 102
NGC 3184	178.336	55.638	14.4	Ferrarese et al. (2000)	SINGS <sup>e</sup>	...	3, 548

<sup>a</sup>H $\alpha$  luminosity from Kennicutt et al. (2008) are converted to star formation rate (SFR) following Equation 2 of Kennicutt (1998).

<sup>b</sup>IRAC 3.6 – 8.0  $\mu\text{m}$  from (Barmby et al. 2006) and MIP 24  $\mu\text{m}$  from Gordon et al. (2006).

<sup>c</sup>See Lewis et al. (2015) for a detailed discussion of M 31’s recent star formation history.

<sup>d</sup>ocal Volume Legacy Survey (LVL, Dale et al. 2009).

<sup>e</sup>*Spitzer* Infrared Nearby Galaxies Survey (SINGS, Kennicutt et al. 2003).

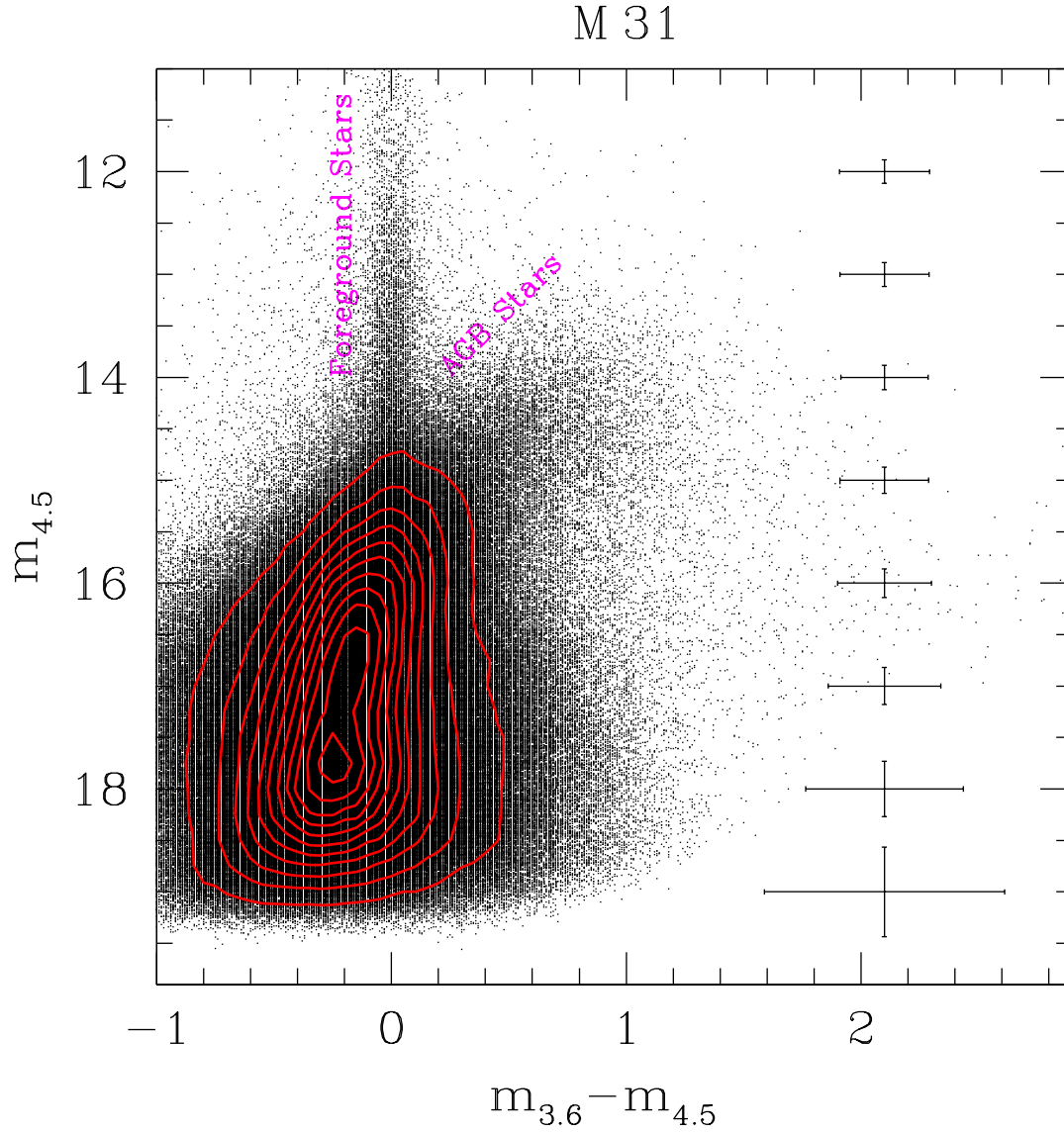


Fig. 1.— The  $m_{4.5}$  vs.  $m_{3.6} - m_{4.5}$  color magnitude diagram (CMD) for the cataloged sources in M31. The red lines represent isodensity contours, and the error bars show mean  $1\sigma$  color and magnitude uncertainties for cataloged sources in 1 magnitude bins.

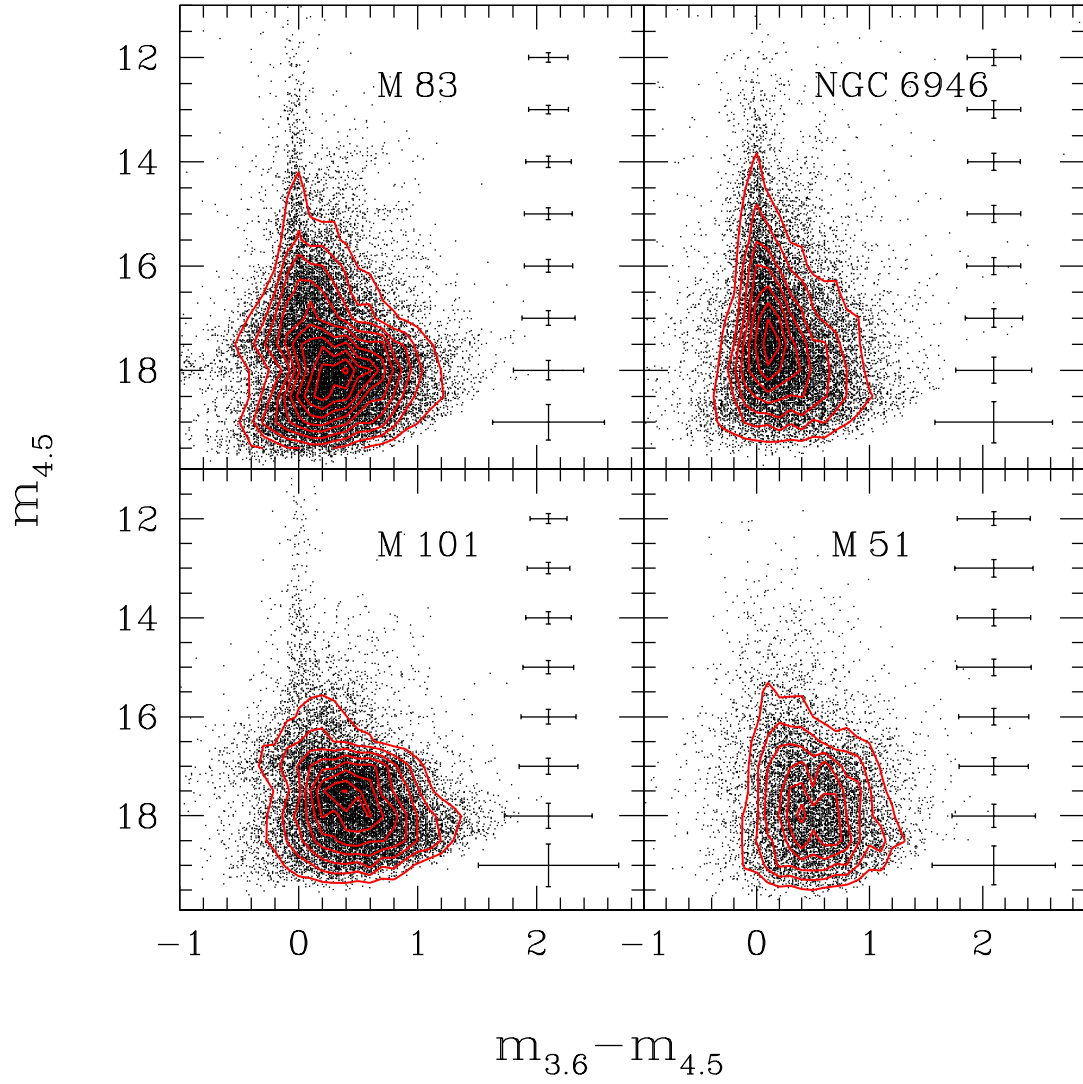


Fig. 2.— Same as Figure 1 for the galaxies M 51, M 83, M 101 and NGC 6946.

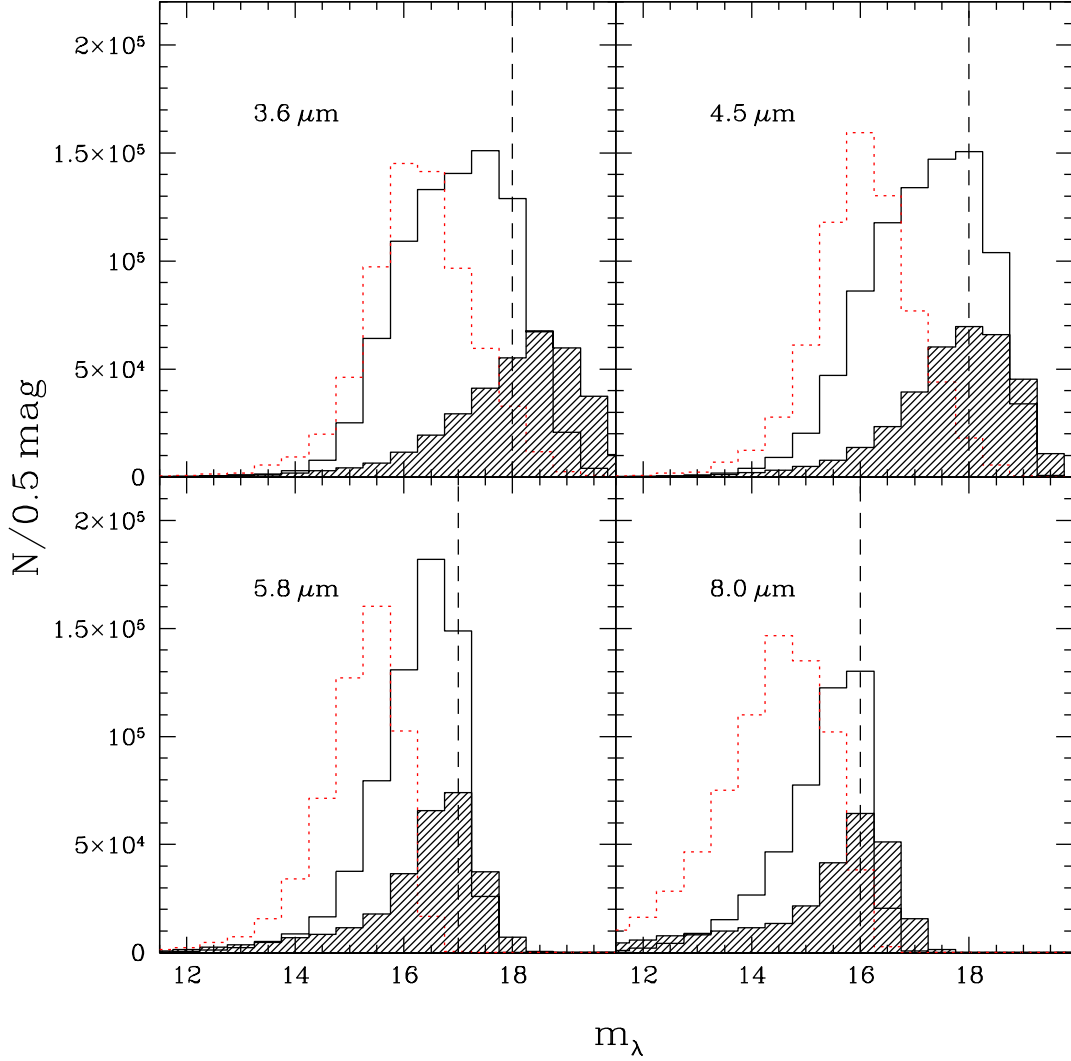


Fig. 3.— Apparent magnitude histograms for all cataloged sources in M31 and in the other 15 galaxies (shaded regions), with the latter scaled up for clarity by a factor of 3. The dotted lines show the apparent-magnitude histograms of the SDWFS catalog sources, scaled up for clarity by a factor of 30 for  $m_{3.6}$  and  $m_{4.5}$ , and by a factor of 50 for  $m_{5.8}$  and  $m_{8.0}$ .

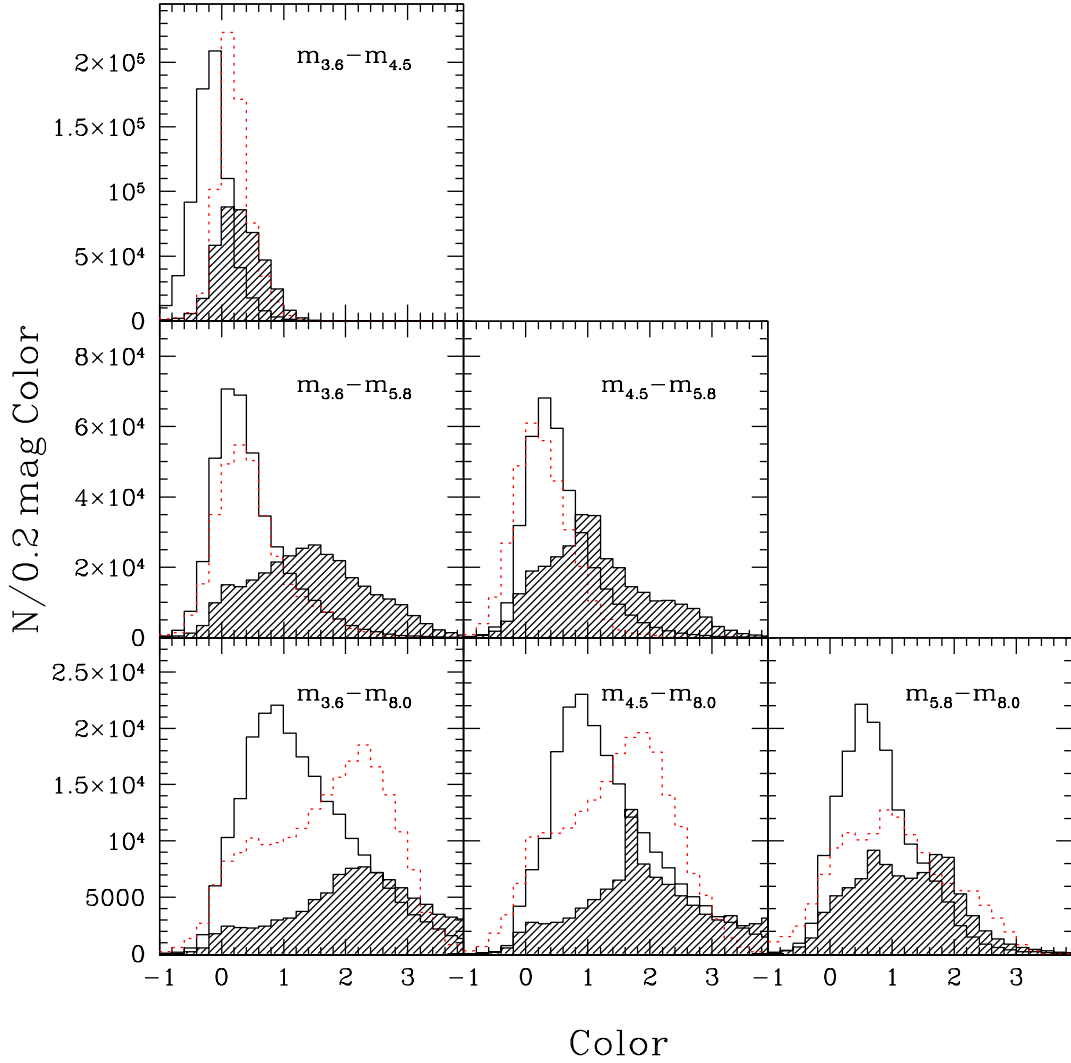


Fig. 4.— Mid-IR color histograms for all cataloged sources in M31 and in the other 15 galaxies (shaded regions) with  $1\sigma$  uncertainty in color  $\lesssim 0.2$ , with the latter scaled up for clarity by factors of 5 (first and second rows) and 2 (bottom row). The dotted lines show the mid-IR color histograms of the SDWFS catalog sources, scaled-up for clarity by factors of 30 (first and second rows) and 15 (bottom row).

Table 2: Catalog for 859, 165 Point Sources in M31

RA (deg)	Dec (deg)	$m_{3.6}$ (mag)	$\sigma_{3.6}$	$\delta_{3.6}$	$m_{4.5}$ (mag)	$\sigma_{4.5}$	$\delta_{4.5}$	$m_{5.8}$ (mag)	$\sigma_{5.8}$	$\delta_{5.8}$	$m_{8.0}$ (mag)	$\sigma_{8.0}$	$\delta_{8.0}$	$m_{24}$ (mag)	$\sigma_{24}$
...	...	...	...	...	...	...	...	...	...	...	...	...	...	...	...
11.48283	42.63817	10.01	0.03	0.10	9.68	0.04	-0.01	9.57	0.03	-0.12	9.54	0.03	0.03	9.72	0.04
11.54072	41.57872	10.46	0.13	0.83	9.69	0.08	1.02	6.79	0.01	99.99	9.53	0.16	2.45	6.18	0.01
10.56790	41.51002	10.12	0.10	1.01	9.70	0.06	0.86	8.30	0.01	99.99	8.32	0.03	0.09	8.08	0.01
10.26228	41.57781	10.00	0.04	0.06	9.71	0.04	-0.01	9.65	0.03	-0.05	9.89	0.06	0.21	9.71	0.04
10.01774	42.00484	10.02	0.01	0.11	9.71	0.02	0.01	9.66	0.03	-0.18	9.70	0.03	0.03	9.61	0.02
...	...	...	...	...	...	...	...	...	...	...	...	...	...	...	...

Table 3: Catalog for 3, 794 Point Sources in NGC 3077

RA (deg)	Dec (deg)	$m_{3.6}$ (mag)	$\sigma_{3.6}$	$\delta_{3.6}$	$m_{4.5}$ (mag)	$\sigma_{4.5}$	$\delta_{4.5}$	$m_{5.8}$ (mag)	$\sigma_{5.8}$	$\delta_{5.8}$	$m_{8.0}$ (mag)	$\sigma_{8.0}$	$\delta_{8.0}$	$m_{24}$ (mag)	$\sigma_{24}$
...	...	...	...	...	...	...	...	...	...	...	...	...	...	...	...
150.81010	68.73050	16.25	0.10	0.49	16.45	0.11	0.81	14.73	0.07	99.99	13.46	0.12	99.99	8.40	0.02
150.53804	68.81851	16.28	0.07	-0.04	16.45	0.07	0.15	16.52	0.14	-0.07	15.47	0.05	-0.57	99.99	99.99
150.82225	68.74129	16.49	0.09	0.30	16.45	0.12	99.99	16.21	0.13	1.27	13.62	0.12	99.99	8.16	0.17
150.86320	68.69979	17.13	0.07	0.47	16.45	0.06	0.17	16.21	0.05	-0.55	15.79	0.11	-0.87	12.87	0.20
150.99858	68.69220	17.14	0.11	0.70	16.46	0.06	0.17	16.36	0.10	0.35	15.42	0.06	0.05	11.33	0.08
...	...	...	...	...	...	...	...	...	...	...	...	...	...	...	...

Table 4: Catalog for 6,972 Point Sources in NGC 1313

RA (deg)	Dec (deg)	$m_{3.6}$ (mag)	$\sigma_{3.6}$	$\delta_{3.6}$	$m_{4.5}$ (mag)	$\sigma_{4.5}$	$\delta_{4.5}$	$m_{5.8}$ (mag)	$\sigma_{5.8}$	$\delta_{5.8}$	$m_{8.0}$ (mag)	$\sigma_{8.0}$	$\delta_{8.0}$	$m_{24}$ (mag)	$\sigma_{24}$
...	...	...	...	...	...	...	...	...	...	...	...	...	...	...	...
49.77658	-66.41660	15.55	0.05	0.00	15.60	0.06	0.01	15.65	0.05	0.23	15.80	0.04	0.11	12.13	0.07
49.56655	-66.49622	15.60	0.12	0.13	15.60	0.13	-0.03	14.38	0.08	99.99	13.28	0.07	99.99	8.47	0.29
49.57424	-66.47501	16.41	0.13	0.08	15.60	0.02	-0.00	14.82	0.04	0.30	13.92	0.06	0.74	8.44	0.04
49.55194	-66.50012	16.43	0.06	0.18	15.61	0.05	0.07	14.91	0.02	0.16	13.72	0.05	0.39	11.58	99.99
49.56185	-66.49652	15.52	0.04	0.01	15.61	0.05	0.10	14.88	0.05	0.54	14.04	0.08	1.28	8.42	0.07
...	...	...	...	...	...	...	...	...	...	...	...	...	...	...	...

Table 5: Catalog for 10,264 Point Sources in NGC 4736 (M94)

RA (deg)	Dec (deg)	$m_{3.6}$ (mag)	$\sigma_{3.6}$	$\delta_{3.6}$	$m_{4.5}$ (mag)	$\sigma_{4.5}$	$\delta_{4.5}$	$m_{5.8}$ (mag)	$\sigma_{5.8}$	$\delta_{5.8}$	$m_{8.0}$ (mag)	$\sigma_{8.0}$	$\delta_{8.0}$	$m_{24}$ (mag)	$\sigma_{24}$
...	...	...	...	...	...	...	...	...	...	...	...	...	...	...	...
192.70675	41.13108	15.65	0.09	0.78	15.11	0.11	0.46	13.03	0.13	0.80	12.19	0.14	1.80	6.20	0.01
192.80644	41.16393	15.38	0.08	0.12	15.11	0.04	0.12	15.34	0.04	0.28	15.04	0.06	0.35	12.35	0.26
192.79610	41.14728	16.13	0.06	0.15	15.11	0.03	0.05	14.38	0.06	-0.00	13.50	0.03	0.07	9.87	0.03
192.73827	41.11505	15.44	0.12	1.36	15.11	0.12	1.19	12.88	0.10	1.02	11.62	0.07	1.79	5.57	0.06
192.70926	41.19135	15.14	0.09	1.11	15.12	0.08	1.24	15.07	0.09	1.64	12.09	0.08	0.99	8.28	0.01
...	...	...	...	...	...	...	...	...	...	...	...	...	...	...	...



Table 6: Catalog for 5, 137 Point Sources in NGC 4826(M 64)

RA (deg)	Dec (deg)	$m_{3.6}$ (mag)	$\sigma_{3.6}$	$\delta_{3.6}$	$m_{4.5}$ (mag)	$\sigma_{4.5}$	$\delta_{4.5}$	$m_{5.8}$ (mag)	$\sigma_{5.8}$	$\delta_{5.8}$	$m_{8.0}$ (mag)	$\sigma_{8.0}$	$\delta_{8.0}$	$m_{24}$ (mag)	$\sigma_{24}$
...	...	...	...	...	...	...	...	...	...	...	...	...	...	...	...
194.06033	21.73660	15.41	0.10	0.13	15.34	0.08	0.07	15.73	0.16	0.73	15.02	0.11	-0.10	11.52	0.05
194.05749	21.67165	16.50	0.05	0.04	15.35	0.10	-0.16	14.36	0.06	-0.04	12.90	0.05	-0.14	9.68	0.03
194.21598	21.66067	15.31	0.06	-0.14	15.36	0.07	-0.02	15.33	0.05	-0.04	15.40	0.08	-0.41	13.06	99.99
194.16860	21.68549	15.37	0.13	99.99	15.37	0.13	99.99	13.62	0.10	0.59	11.61	0.09	0.49	6.93	0.03
194.12018	21.64330	15.51	0.07	0.33	15.38	0.07	0.37	14.95	0.10	0.26	14.09	0.05	-0.02	10.57	0.07
...	...	...	...	...	...	...	...	...	...	...	...	...	...	...	...

Table 7: Catalog for 23, 331 Point Sources in NGC 5236 (M 83)

RA (deg)	Dec (deg)	$m_{3.6}$ (mag)	$\sigma_{3.6}$	$\delta_{3.6}$	$m_{4.5}$ (mag)	$\sigma_{4.5}$	$\delta_{4.5}$	$m_{5.8}$ (mag)	$\sigma_{5.8}$	$\delta_{5.8}$	$m_{8.0}$ (mag)	$\sigma_{8.0}$	$\delta_{8.0}$	$m_{24}$ (mag)	$\sigma_{24}$
...	...	...	...	...	...	...	...	...	...	...	...	...	...	...	...
204.15718	-29.85278	13.49	0.04	-0.03	13.54	0.03	-0.01	13.49	0.02	-0.05	13.57	0.05	0.25	11.95	99.99
204.15082	-29.74423	13.50	0.03	-0.03	13.55	0.02	-0.01	13.52	0.03	-0.01	13.55	0.02	-0.05	11.89	99.99
204.23002	-29.97769	13.75	0.06	0.05	13.55	0.03	-0.08	13.64	0.02	0.01	13.89	0.04	0.03	12.31	99.99
204.22073	-29.86514	14.09	0.09	0.93	13.55	0.08	0.75	10.94	0.05	0.77	8.38	0.03	99.99	4.18	0.03
204.18453	-29.87696	13.57	0.04	-0.01	13.56	0.04	-0.05	13.15	0.05	0.18	12.74	0.09	0.95	9.07	99.99
...	...	...	...	...	...	...	...	...	...	...	...	...	...	...	...

Table 8: Catalog for 5,617 Point Sources in NGC 5068

RA (deg)	Dec (deg)	$m_{3.6}$ (mag)	$\sigma_{3.6}$	$\delta_{3.6}$	$m_{4.5}$ (mag)	$\sigma_{4.5}$	$\delta_{4.5}$	$m_{5.8}$ (mag)	$\sigma_{5.8}$	$\delta_{5.8}$	$m_{8.0}$ (mag)	$\sigma_{8.0}$	$\delta_{8.0}$	$m_{24}$ (mag)	$\sigma_{24}$
...	...	...	...	...	...	...	...	...	...	...	...	...	...	...	...
199.72607	-21.03384	15.92	0.14	0.83	15.41	0.11	0.37	13.75	0.11	0.71	11.39	0.04	0.23	7.91	0.07
199.73146	-21.04449	15.61	0.13	0.05	15.41	0.09	-0.10	13.50	0.09	-0.03	11.48	0.02	-0.04	7.87	0.11
199.70099	-20.97649	15.48	0.13	0.88	15.42	0.13	0.85	14.22	0.11	0.88	11.91	0.06	0.64	8.32	0.02
199.73044	-21.04431	15.22	0.14	0.23	15.43	0.12	0.40	13.26	0.11	0.08	11.00	0.04	-0.38	7.89	0.05
199.71533	-21.07158	15.37	0.05	0.02	15.43	0.04	0.02	15.08	0.07	-0.38	13.84	0.07	0.37	9.70	0.05
...	...	...	...	...	...	...	...	...	...	...	...	...	...	...	...

Table 9: Catalog for 15,813 Point Sources in NGC 6946

RA (deg)	Dec (deg)	$m_{3.6}$ (mag)	$\sigma_{3.6}$	$\delta_{3.6}$	$m_{4.5}$ (mag)	$\sigma_{4.5}$	$\delta_{4.5}$	$m_{5.8}$ (mag)	$\sigma_{5.8}$	$\delta_{5.8}$	$m_{8.0}$ (mag)	$\sigma_{8.0}$	$\delta_{8.0}$	$m_{24}$ (mag)	$\sigma_{24}$
...	...	...	...	...	...	...	...	...	...	...	...	...	...	...	...
308.65553	60.13594	14.78	0.06	-0.11	14.59	0.06	-0.30	14.40	0.04	99.99	13.56	0.24	99.99	8.21	0.26
308.94799	59.96213	14.44	0.16	-0.02	14.60	0.14	0.13	14.36	0.09	-0.02	14.42	0.15	0.06	99.99	99.99
308.64470	60.09664	14.57	0.04	-0.06	14.60	0.04	0.00	14.38	0.05	-0.03	14.20	0.04	-0.23	11.33	99.99
308.81946	60.18289	14.80	0.14	0.93	14.60	0.10	1.15	12.19	0.10	1.13	11.01	0.12	1.71	5.14	0.01
309.03955	60.09698	13.45	0.11	0.56	14.60	0.10	0.67	12.25	0.12	0.59	12.32	99.99	99.99	99.99	99.99
...	...	...	...	...	...	...	...	...	...	...	...	...	...	...	...

Table 10: Catalog for 991 Point Sources in NGC 5474

RA (deg)	Dec (deg)	$m_{3.6}$ (mag)	$\sigma_{3.6}$	$\delta_{3.6}$	$m_{4.5}$ (mag)	$\sigma_{4.5}$	$\delta_{4.5}$	$m_{5.8}$ (mag)	$\sigma_{5.8}$	$\delta_{5.8}$	$m_{8.0}$ (mag)	$\sigma_{8.0}$	$\delta_{8.0}$	$m_{24}$ (mag)	$\sigma_{24}$
...	...	...	...	...	...	...	...	...	...	...	...	...	...	...	...
211.20194	53.64062	18.02	0.05	0.06	17.17	0.07	-0.19	16.70	0.11	99.99	16.18	0.12	0.49	11.28	0.05
211.29572	53.67260	17.25	0.06	0.02	17.17	0.06	0.06	16.88	0.08	-0.09	15.81	0.12	-0.43	11.49	0.05
211.25098	53.63765	18.05	0.16	1.14	17.18	0.13	0.80	16.08	0.09	0.49	14.49	0.07	0.42	10.31	0.06
211.23574	53.66682	17.37	0.05	-0.07	17.19	0.04	-0.02	16.71	0.17	-0.32	15.94	0.11	0.80	11.06	0.09
211.29303	53.71026	17.28	0.08	-0.03	17.21	0.13	0.45	17.16	0.15	-0.25	16.12	0.23	0.22	12.94	0.27
...	...	...	...	...	...	...	...	...	...	...	...	...	...	...	...

Table 11: Catalog for 16, 291 Point Sources in NGC 5457 (M 101)

RA (deg)	Dec (deg)	$m_{3.6}$ (mag)	$\sigma_{3.6}$	$\delta_{3.6}$	$m_{4.5}$ (mag)	$\sigma_{4.5}$	$\delta_{4.5}$	$m_{5.8}$ (mag)	$\sigma_{5.8}$	$\delta_{5.8}$	$m_{8.0}$ (mag)	$\sigma_{8.0}$	$\delta_{8.0}$	$m_{24}$ (mag)	$\sigma_{24}$
...	...	...	...	...	...	...	...	...	...	...	...	...	...	...	...
210.78059	54.33504	14.36	0.09	0.01	14.33	0.07	0.01	14.38	0.03	-0.43	14.72	0.09	99.99	11.05	99.99
210.67501	54.19461	14.28	0.05	0.00	14.34	0.04	0.01	14.55	0.05	0.10	14.25	0.05	0.06	11.79	0.19
210.77003	54.32386	14.48	0.10	0.62	14.35	0.14	0.90	11.57	0.06	0.57	9.73	0.02	0.51	5.45	0.01
210.86363	54.31284	14.77	0.09	0.43	14.35	0.06	0.38	12.01	0.07	0.51	10.21	0.03	0.58	5.41	0.01
210.58743	54.46138	14.12	0.07	-0.07	14.35	0.06	0.12	14.33	0.06	0.07	14.15	0.03	-0.06	12.01	0.29
...	...	...	...	...	...	...	...	...	...	...	...	...	...	...	...

Table 12: Catalog for 4,321 Point Sources in NGC 45

RA (deg)	Dec (deg)	$m_{3.6}$ (mag)	$\sigma_{3.6}$	$\delta_{3.6}$	$m_{4.5}$ (mag)	$\sigma_{4.5}$	$\delta_{4.5}$	$m_{5.8}$ (mag)	$\sigma_{5.8}$	$\delta_{5.8}$	$m_{8.0}$ (mag)	$\sigma_{8.0}$	$\delta_{8.0}$	$m_{24}$ (mag)	$\sigma_{24}$
...	...	...	...	...	...	...	...	...	...	...	...	...	...	...	...
3.63601	-23.18667	15.84	0.06	0.31	15.96	0.09	0.77	15.71	0.17	0.61	14.63	0.05	0.76	10.74	0.09
3.40049	-23.19893	16.25	0.07	0.10	15.96	0.13	0.39	15.29	0.07	-0.18	12.62	0.03	0.13	9.38	0.03
3.48302	-23.23012	16.11	0.08	0.22	15.96	0.05	0.35	16.26	0.07	0.68	15.41	0.06	0.70	11.39	0.13
3.54977	-23.14415	16.34	0.07	0.19	15.97	0.09	0.10	16.12	0.09	0.09	15.33	0.04	-0.22	11.63	0.18
3.66439	-23.20038	16.05	0.04	0.10	15.97	0.09	-0.00	16.33	0.11	0.53	15.10	0.09	99.99	11.59	99.99
...	...	...	...	...	...	...	...	...	...	...	...	...	...	...	...

Table 13: Catalog for 8,601 Point Sources in NGC 5194 (M 51)

RA (deg)	Dec (deg)	$m_{3.6}$ (mag)	$\sigma_{3.6}$	$\delta_{3.6}$	$m_{4.5}$ (mag)	$\sigma_{4.5}$	$\delta_{4.5}$	$m_{5.8}$ (mag)	$\sigma_{5.8}$	$\delta_{5.8}$	$m_{8.0}$ (mag)	$\sigma_{8.0}$	$\delta_{8.0}$	$m_{24}$ (mag)	$\sigma_{24}$
...	...	...	...	...	...	...	...	...	...	...	...	...	...	...	...
202.52413	47.26076	14.32	0.11	0.68	13.58	0.06	-0.01	13.43	0.08	0.02	13.61	0.05	0.50	11.08	0.19
202.46449	47.19562	13.53	0.14	0.59	13.58	0.11	-0.09	12.37	0.09	-0.19	11.49	0.07	0.96	6.96	0.17
202.48110	47.19441	14.27	0.14	-1.19	13.59	0.08	-0.82	11.41	0.09	0.04	9.61	0.08	0.11	5.43	0.17
202.48202	47.19663	14.19	0.09	0.39	13.59	0.05	0.04	13.08	0.11	1.11	10.32	0.11	-0.13	4.76	0.06
202.46688	47.21179	14.03	0.13	0.57	13.64	0.06	0.66	11.39	0.11	0.71	9.82	0.06	0.96	4.65	0.03
...	...	...	...	...	...	...	...	...	...	...	...	...	...	...	...

Table 14: Catalog for 5,579 Point Sources in NGC 2903

RA (deg)	Dec (deg)	$m_{3.6}$ (mag)	$\sigma_{3.6}$	$\delta_{3.6}$	$m_{4.5}$ (mag)	$\sigma_{4.5}$	$\delta_{4.5}$	$m_{5.8}$ (mag)	$\sigma_{5.8}$	$\delta_{5.8}$	$m_{8.0}$ (mag)	$\sigma_{8.0}$	$\delta_{8.0}$	$m_{24}$ (mag)	$\sigma_{24}$
...	...	...	...	...	...	...	...	...	...	...	...	...	...	...	...
143.03345	21.47890	14.79	0.09	0.78	14.53	0.12	0.56	11.80	0.10	0.46	9.94	0.03	0.45	6.05	0.06
142.92413	21.63127	14.47	0.06	-0.00	14.53	0.06	0.03	14.61	0.07	-0.01	14.41	0.08	-0.35	11.75	0.25
143.04889	21.51972	14.85	0.11	0.34	14.53	0.13	0.11	12.76	0.10	0.10	10.68	0.06	0.04	7.46	0.11
142.93511	21.64432	14.49	0.04	-0.02	14.54	0.11	-0.02	14.80	0.09	0.01	14.12	0.04	-0.45	12.26	99.99
142.84140	21.53222	14.60	0.10	99.99	14.54	0.12	99.99	15.95	0.13	0.67	14.35	0.05	99.99	11.30	99.99
...	...	...	...	...	...	...	...	...	...	...	...	...	...	...	...

Table 15: Catalog for 4,217 Point Sources in NGC 925

RA (deg)	Dec (deg)	$m_{3.6}$ (mag)	$\sigma_{3.6}$	$\delta_{3.6}$	$m_{4.5}$ (mag)	$\sigma_{4.5}$	$\delta_{4.5}$	$m_{5.8}$ (mag)	$\sigma_{5.8}$	$\delta_{5.8}$	$m_{8.0}$ (mag)	$\sigma_{8.0}$	$\delta_{8.0}$	$m_{24}$ (mag)	$\sigma_{24}$
...	...	...	...	...	...	...	...	...	...	...	...	...	...	...	...
36.82781	33.63954	15.73	0.07	-0.01	15.67	0.10	-0.01	15.66	0.06	-0.25	15.39	0.07	-0.85	11.90	0.28
36.84670	33.52045	15.99	0.09	1.12	15.67	0.12	1.00	15.64	0.07	0.93	14.38	0.06	1.40	10.47	0.07
36.82457	33.57855	15.79	0.11	0.28	15.68	0.13	0.48	14.56	0.14	1.16	12.45	0.10	0.72	7.79	0.10
36.92907	33.68388	15.63	0.06	0.00	15.68	0.09	0.00	15.94	0.11	-0.42	15.12	0.14	-0.56	99.99	99.99
36.93849	33.57978	15.93	0.05	0.15	15.68	0.09	0.10	15.61	0.09	-0.01	14.26	0.05	-0.02	11.85	0.12
...	...	...	...	...	...	...	...	...	...	...	...	...	...	...	...

Table 16: Catalog for 3,102 Point Sources in NGC 3627

RA (deg)	Dec (deg)	$m_{3.6}$ (mag)	$\sigma_{3.6}$	$\delta_{3.6}$	$m_{4.5}$ (mag)	$\sigma_{4.5}$	$\delta_{4.5}$	$m_{5.8}$ (mag)	$\sigma_{5.8}$	$\delta_{5.8}$	$m_{8.0}$ (mag)	$\sigma_{8.0}$	$\delta_{8.0}$	$m_{24}$ (mag)	$\sigma_{24}$
...	...	...	...	...	...	...	...	...	...	...	...	...	...	...	...
170.09283	12.88126	14.40	0.04	0.09	13.75	0.10	0.09	13.03	0.06	0.03	12.14	0.04	-0.03	8.28	0.01
170.05499	13.00885	13.79	0.16	-0.09	13.76	0.13	0.15	11.11	0.11	0.02	9.52	0.10	0.21	4.51	0.05
170.06840	12.96378	14.03	0.13	1.36	13.76	0.12	1.54	11.51	0.13	1.71	9.79	0.08	1.85	3.68	0.01
170.01328	12.92316	13.89	0.05	-0.02	13.80	0.09	-0.05	13.86	0.05	0.10	13.61	0.06	-0.21	13.06	99.99
170.05455	13.00498	14.12	0.10	0.15	13.81	0.12	0.24	11.63	0.08	99.99	9.71	0.08	99.99	4.78	0.09
...	...	...	...	...	...	...	...	...	...	...	...	...	...	...	...

Table 17: Catalog for 3,548 Point Sources in NGC 3184

RA (deg)	Dec (deg)	$m_{3.6}$ (mag)	$\sigma_{3.6}$	$\delta_{3.6}$	$m_{4.5}$ (mag)	$\sigma_{4.5}$	$\delta_{4.5}$	$m_{5.8}$ (mag)	$\sigma_{5.8}$	$\delta_{5.8}$	$m_{8.0}$ (mag)	$\sigma_{8.0}$	$\delta_{8.0}$	$m_{24}$ (mag)	$\sigma_{24}$
...	...	...	...	...	...	...	...	...	...	...	...	...	...	...	...
154.53453	41.39239	16.82	0.10	0.22	16.13	0.06	0.13	15.70	0.06	0.04	14.37	0.12	-0.14	10.91	0.14
154.63606	41.39248	16.35	0.09	0.19	16.13	0.04	0.10	16.29	0.07	0.46	15.34	0.07	-0.50	12.46	99.99
154.67640	41.38895	16.47	0.12	0.29	16.14	0.09	0.21	15.76	0.09	0.33	14.63	0.05	-0.22	99.99	99.99
154.56665	41.44029	16.09	0.12	0.39	16.15	0.12	0.71	13.72	0.11	0.87	11.16	0.03	0.32	7.93	0.06
154.39740	41.38107	16.75	0.15	1.08	16.15	0.08	0.79	15.20	0.19	99.99	14.70	0.27	0.02	99.99	99.99
...	...	...	...	...	...	...	...	...	...	...	...	...	...	...	...